Beam focusing by near-field transition radiation

S Corde, M Gilljohann, X Davoine, L Gremillet, A Sampath, M Tamburini

Beam focusing by near-field transition radiation

S. Corde[1], M. Gilljohann[1], X. Davoine[2], L. Gremillet[2], A. Sampath[3], and M. Tamburini[3]

[1]IP Paris, France
[2]CEA, France
[3]MPIK, Germany

Contents

1 Introduction

The goal of this document is to assess the possibility to measure and demonstrate a beam focusing effect from near-field coherent transition radiation (NF-CTR) using beam parameters that can be realistically achieved by the FACET-II facility at SLAC in the context of the E-332 experiment "Near-field-CTR-based self-focusing in beam-multifoil collisions: towards solid-density beams, extremely-dense gamma-ray pulses and laserless SFQED".

2 Analytical estimates

2.1 Effective focal length for the beam central slice

In SI units, the self-fields of an ultrarelativistic Gaussian particle beam are essentially transverse, and can be approximated as:

$$E_r^b(r,z,t) = \frac{qN}{(2\pi)^{3/2}\sigma_\parallel \epsilon_0 r}\left(1-e^{-r^2/(2\sigma_\perp^2)}\right) e^{-\frac{(z-vt)^2}{2\sigma_\parallel^2}} \tag{1}$$

$$B_\theta^b(r,z,t) = \frac{qN}{(2\pi)^{3/2}\sigma_\parallel c\epsilon_0 r}\left(1-e^{-r^2/(2\sigma_\perp^2)}\right) e^{-\frac{(z-vt)^2}{2\sigma_\parallel^2}}\ , \tag{2}$$

with $q = -e$ for an electron beam. The beam is taken to be centered at $\xi \equiv z - ct = 0$. We assume that the self-fields are perfectly reflected by the conductor, which is reasonable if $\sigma_\perp \gtrsim \sigma_\parallel$. If the conductor's boundary is located at $z = 0$, the NF-CTR fields can therefore be written as:

$$E_r^c(r,z,t) = -\frac{qN}{(2\pi)^{3/2}\sigma_\parallel \epsilon_0 r}\left(1 - e^{-r^2/(2\sigma_\perp^2)}\right) e^{-\frac{(z+vt)^2}{2\sigma_\parallel^2}} \tag{3}$$

$$B_\theta^c(r,z,t) = \frac{qN}{(2\pi)^{3/2}\sigma_\parallel c\epsilon_0 r}\left(1 - e^{-r^2/(2\sigma_\perp^2)}\right) e^{-\frac{(z+vt)^2}{2\sigma_\parallel^2}}\,, \tag{4}$$

where the superscript c expresses that these fields are induced by the conductor. The above expressions obviously satisfy the boundary conditions at the conductor's surface: $E_r^c(r,0,t) = -E_r^b(r,0,t)$ and $B_\theta^c(r,0,t) = B_\theta^b(r,0,t)$.

We are now interested in the beam evolution in the (x, p_x) phase space. An electron in the central slice of the beam ($z = vt$), and with $x > 0$ and $y = 0$ ($r = x$), thus experiences a transverse momentum kick before hitting the conductor:

$$\begin{aligned}
\Delta p_x &= \int_{-\infty}^{0} q(E_x^c - vB_y^c)\,dt \simeq -2qc\int_{-\infty}^{0} B_\theta^c(r=x, z=vt, t)\,dt \\
&= -\frac{2q^2N}{(2\pi)^{3/2}\epsilon_0\sigma_\parallel x}\left(1 - e^{-x^2/2(\sigma_\perp^2)}\right)\int_{-\infty}^{0} e^{-2(vt/\sigma_\parallel)^2}\,dt \\
&\simeq -\frac{q^2N}{4\pi\epsilon_0 cx}\left(1 - e^{-x^2/(2\sigma_\perp^2)}\right) \\
&\simeq -\frac{q^2Nx}{8\pi\epsilon_0 c\sigma_\perp^2}\,,
\end{aligned} \tag{5}$$

where the last approximation holds for $x \lesssim \sigma_\perp$. From Eq. (5), the angular kick is $\Delta\theta_x \simeq \Delta p_x/p_z \simeq \Delta p_x/(\gamma mc) = -q^2Nx/(8\pi\epsilon_0\sigma_\perp^2\mathcal{E})$, where $\mathcal{E} = \gamma mc^2$ is the particle energy. For a perfect thin lens of focal length f, the angular kick writes $\Delta\theta_x = -x/f$. We thus deduce the effective focal length for the beam central slice of the near-field transition radiation focusing effect:

$$f = \frac{8\pi\epsilon_0\sigma_\perp^2\mathcal{E}}{q^2N} \tag{6}$$

In physical units and for $|q| = e$, this writes:

$$f[\mathrm{mm}] = 0.2225\,\frac{\sigma_\perp[\mu\mathrm{m}]^2\mathcal{E}[\mathrm{GeV}]}{Q[\mathrm{nC}]} \tag{7}$$

Note that the result is independent of the bunch length, because the self fields are inversely proportional to $\sigma_\parallel$ but the focusing effect is integrated over the bunch length. However, by using perfect reflected fields we have assumed $\sigma_\parallel \lesssim \sigma_\perp$, and therefore the bunch length cannot be arbitrarily chosen; it needs to be smaller than the beam size for the desired focal length. Table 1 shows a few examples of focal length values for different beam sizes.

Beam size	Focal length
$30\,\mu$m	1.0 m
$10\,\mu$m	110 mm
$3\,\mu$m	10 mm
$1\,\mu$m	1.1 mm
$0.55\,\mu$m	$340\,\mu$m

Table 1: Examples of focal length values for different beam sizes and for $Q = 2\,\mathrm{nC}$ and $\mathcal{E} = 10\,\mathrm{GeV}$. $0.55\,\mu$m is the beam size value used in A. Sampath *et al.*, Phys. Rev. Lett. 126, 064801 (2021).

2.2 Beam evolution with a single foil

To understand if this foil focusing effect will be measurable, we need to account for the finite beam emittance and the multiple scattering in the foil.

The transport matrix associated to the NF-CTR-induced lens is:

$$M = \begin{pmatrix} 1 & 0 \\ -1/f & 1 \end{pmatrix} \tag{8}$$

and the beam Twiss parameters after experiencing NF-CTR are:

$$\alpha_2 = -M_{11}M_{21}\beta_1 + (M_{11}M_{22} + M_{12}M_{21})\alpha_1 - M_{12}M_{22}\gamma_1 \tag{9}$$
$$\beta_2 = M_{11}^2\beta_1 - 2M_{11}M_{12}\alpha_1 + M_{12}^2\gamma_1 \tag{10}$$

and they simplify to:

$$\alpha_2 = \alpha_1 + \beta_1/f \tag{11}$$
$$\beta_2 = \beta_1 \tag{12}$$

where $(\alpha_1, \beta_1, \gamma_1)$ and $(\alpha_2, \beta_2, \gamma_2)$ are the beam Twiss parameters respectively just before and just after experiencing NF-CTR, and $\gamma_{1,2} = (1 + \alpha_{1,2}^2)/\beta_{1,2}$.

If the waist is initially at the foil ($\alpha_1 = 0$), then the new waist after the beam has experienced NF-CTR is:

$$s^* = \alpha_2\beta_2^* = \frac{\alpha_2\beta_2}{1 + \alpha_2^2} \tag{13}$$
$$= f\,\frac{\beta^2}{\beta^2 + f^2} \tag{14}$$

where $\beta = \beta_2 = \beta_1$. To have a waist shift similar to the focal length ($s^\star \sim f$), one needs $f \ll \beta$.

A second important parameter is the beam divergence. If the beam divergence changes substantially due to NF-CTR, this gives us a way to measure and demonstrate the NF-CTR effect in the experiment. The beam divergence before and after NF-CTR read:

$$\theta_1 = \sqrt{\epsilon_g(1 + \alpha_1^2)/\beta_1} \tag{15}$$
$$\theta_2 = \sqrt{\epsilon_g(1 + \alpha_2^2)/\beta_2} \tag{16}$$

Normalized emittance	β/f
$100\,\mu$m	0.176
$30\,\mu$m	0.586
$10\,\mu$m	1.76
$3\,\mu$m	5.86

Table 2: Examples of values of the figure of merit β/f for different normalized emittances and for $Q = 2\,$nC.

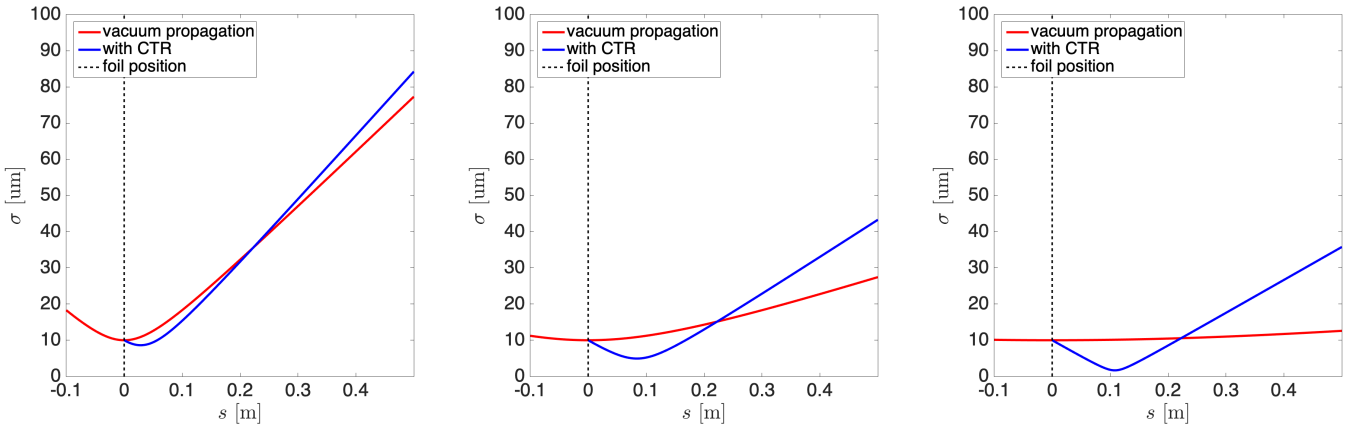

Figure 1: **Beam evolution and focusing effect from near-field transition radiation**. Evolution of the beam size with the propagation distance with and without foil, for normalized emittances of $30\,\mu$m (left), $10\,\mu$m (middle) and $3\,\mu$m (right), and for an initial waist located at the foil position and for a beam size of $10\,\mu$m at the waist. The effect of multiple scattering is not taken into account.

where ϵ_g is the beam geometrical emittance. Again, if the waist is initially at the foil ($\alpha_1 = 0$), then we have:

$$\theta_2 = \theta_1\sqrt{1 + (\beta/f)^2} \tag{17}$$

Similarly to the waist shift, we see that the effect is strong and measurable for $f \ll \beta$.

A good figure of merit to determine whether NF-CTR focusing is measurable is therefore the ratio β/f (for $\beta/f \gtrsim 1$, the effect can easily be demonstrated experimentally). We have:

$$\beta/f = \frac{q^2 N}{8\pi\epsilon_0 mc^2\epsilon_n} = 8.794\,\frac{Q[\text{nC}]}{\epsilon_n[\mu\text{m}]} \tag{18}$$

with $\epsilon_n = \gamma\epsilon_g$ the normalized emittance of the beam. Interestingly, we see that this figure of merit does not depend on the beam size, but only depends on the charge and normalized emittance. Table 2 shows a few examples of values for this figure of merit β/f for different normalized emittances.

Figure 1 shows the evolution of the beam size during propagation with and without the foil, for different normalized emittances. The result shows that for an emittance of $30\,\mu$m, the NF-CTR focusing effect is measurable, but to use it to reach significantly smaller beam size at the new waist, an emittance of $3\,\mu$m is much more promising.

2.3 Effect of multiple scattering

Multiple scattering in the foil can be detrimental in increasing the angular spread and emittance of the beam, and in preventing its focusing to very small spot size at the new waist. The rms scattering angle due to multiple scattering in the foil writes (see The Review of Particle Physics (2020), P.A. Zyla et al. (Particle Data Group), Prog. Theor. Exp. Phys. 2020, 083C01 (2020), section 34.3 Multiple scattering through small angles):

$$\theta_s = \frac{13.6}{\mathcal{E}[\mathrm{MeV}]}\sqrt{d/X_0}\,[1 + 0.038\ln(d/X_0)] \tag{19}$$

where X_0 is the radiation length of the material and d its thickness. For aluminum, $X_0 = 8.897\,\mathrm{cm}$. Table 3 shows a few examples of scattering angle values for an aluminum foil and for different thicknesses.

To assess the importance of this multiple scattering effect, the scattering angle should be compared to $\sqrt{\epsilon_g/\beta}$, where $\beta = \beta_2 = \beta_1$ is the beta function before multiple scattering. If the waist is located at the foil, $\alpha_1 = 0$ and $\sqrt{\epsilon_g/\beta}$ corresponds to the beam divergence θ_1, before the beam has experienced NF-CTR.

For a beam size of $10\,\mu\mathrm{m}$ and a normalized emittance of $30\,\mu\mathrm{m}$, $\theta_1 = 153\,\mu\mathrm{rad}$. In this case, even for a 100-μm-thick Al foil, multiple scattering will not compromise our ability to demonstrate NF-CTR focusing, the increase in beam divergence is still dominated by NF-CTR, see Fig. 2 and Table 4.

For a beam size of $10\,\mu\mathrm{m}$ and a normalized emittance of $3\,\mu\mathrm{m}$, $\theta_1 = 15.3\,\mu\mathrm{rad}$. In this case, a 100-$\mu$m-thick Al foil will significantly limit our capability to focus the beam to very small spot sizes using NF-CTR. A micrometer-thick Al foil is thus desired in this case. Indeed, in Fig. 3, we see that for an Al thickness of $100\,\mu\mathrm{m}$, multiple scattering considerably increases the spot size at the new waist, by more than a factor of 2. For an Al thickness of $10\,\mu\mathrm{m}$, a weak effect is still visible, while for $1\,\mu\mathrm{m}$ thickness the curves with or without multiple scattering overlap.

Al thickness	Scattering angle (rms)
$100\,\mu\mathrm{m}$	$34\,\mu\mathrm{rad}$
$10\,\mu\mathrm{m}$	$9.4\,\mu\mathrm{rad}$
$1\,\mu\mathrm{m}$	$2.6\,\mu\mathrm{rad}$
$0.5\,\mu\mathrm{m}$	$1.7\,\mu\mathrm{rad}$

Table 3: Examples of scattering angle values for $\mathcal{E} = 10\,\mathrm{GeV}$ and for an aluminum foil of different thicknesses. $0.5\,\mu\mathrm{m}$ is the Al thickness used in A. Sampath *et al.*, Phys. Rev. Lett. 126, 064801 (2021).

Conditions	Beam divergence (rms)
No foil	$153\,\mu\mathrm{rad}$
NF-CTR only	$178\,\mu\mathrm{rad}$
Multiple scattering only	$157\,\mu\mathrm{rad}$
NF-CTR + multiple scattering	$181\,\mu\mathrm{rad}$

Table 4: Beam divergence for different conditions. Here the beam parameters are the same as for Fig. 2: the normalized emittance is $30\,\mu\mathrm{m}$, the beam size is $10\,\mu\mathrm{m}$, the charge is $2\,\mathrm{nC}$, the beam energy is $10\,\mathrm{GeV}$, and the Al foil has a thickness of $100\,\mu\mathrm{m}$.

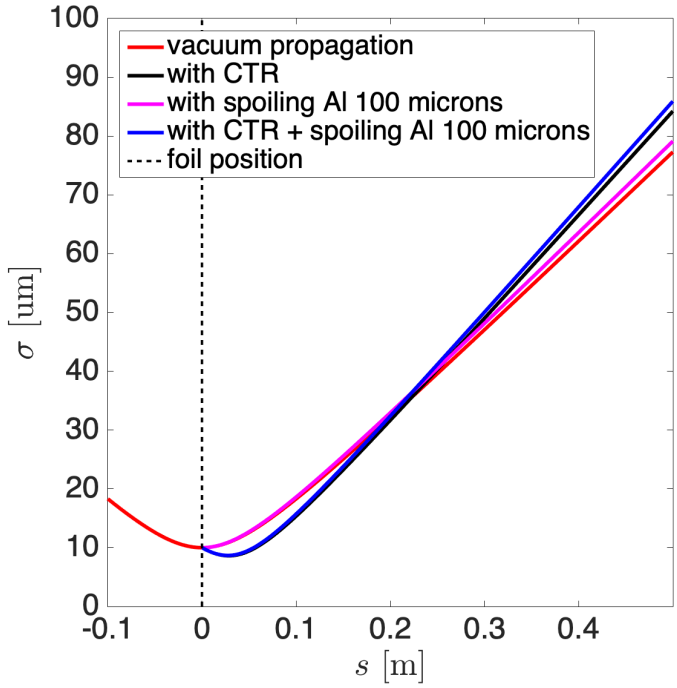

Figure 2: **Beam evolution with multiple scattering included and** $30\,\mu$m **normalized emittance**. Evolution of the beam size with the propagation distance with and without foil, for an initial waist located at the foil position and for a beam size of $10\,\mu$m at the waist. The effect of multiple scattering is taken into account for an aluminum foil of $100\,\mu$m thickness.

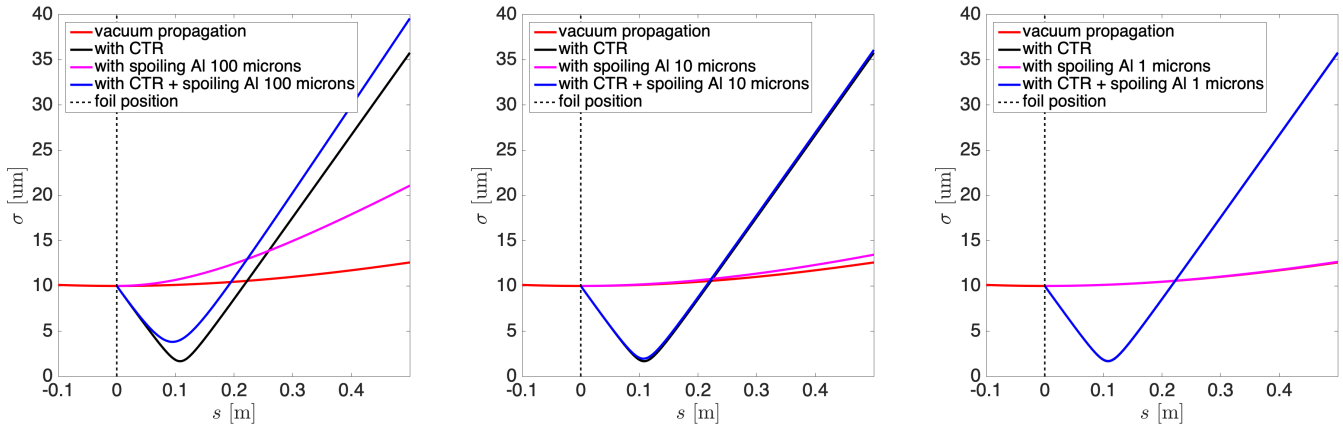

Figure 3: **Beam evolution with multiple scattering included and** $3\,\mu$m **normalized emittance**. Evolution of the beam size with the propagation distance with and without foil, for an initial waist located at the foil position and for a beam size of $10\,\mu$m at the waist. The effect of multiple scattering is taken into account for an aluminum foil with a thickness of $100\,\mu$m (left), $10\,\mu$m (middle) and $1\,\mu$m (right).

2.4 Estimates of energy deposited in foil

One possible limitation to the E-332 experiment could arise from a large damage of the foil after each foil. Several effects can contribute to the foil damage. Here we do

not account for effects that could arise from the mechanical momentum transferred to the foil or the energy deposed in the foil due to ionization. We estimate the energy deposited in the foil solely from the resistive current driven in the foil surface and bulk.

In the bulk, the plasma return current is obtained simply as $\mathbf{j}_p = -\mathbf{j}_b$ ($\mathbf{j}_p$ plasma current, $\mathbf{j}_b$ beam current), and the energy deposited in a volume dV and in a time dt writes as:

$$dW = \mathbf{j}_p \cdot \mathbf{E}\, dV dt = \frac{|\mathbf{j}_b|^2}{\sigma_{\mathrm{Al}}}\, dV dt \tag{20}$$

where σ_{Al} is the conductivity of the aluminum foil. With $c_v = C_v/V$ the specific heat capacity per unit volume, one can estimate the local increase in temperature in the bulk by:

$$\Delta T = \int \frac{|\mathbf{j_b}|^2}{c_v \sigma_{\mathrm{Al}}}\, dt \tag{21}$$

with $|\mathbf{j}_b| = \frac{ecN}{(2\pi)^{3/2}\sigma_\parallel \sigma_\perp^2} e^{-(z-vt)^2/(2\sigma_\parallel^2)} e^{-r^2/(2\sigma_\perp^2)}$. The maximum temperature increase is on axis ($r = 0$) and reads:

$$\Delta T_{\max} = \frac{e^2 c N^2}{8\pi^{5/2}\sigma_\parallel \sigma_\perp^4} \frac{1}{c_v \sigma_{\mathrm{Al}}} \tag{22}$$

We consider a beam charge of 2 nC and we consider first the following estimates for solid aluminum at room temperature in static condition: $c_v = 2.4 \times 10^6\,\mathrm{J\,m^{-3}\,K^{-1}}$ and $\sigma_{\mathrm{Al}} = 4 \times 10^7\,\Omega^{-1}\,\mathrm{m}^{-1}$. For $\sigma_\parallel = \sigma_\perp = 5\,\mu$m, it gives $\Delta T_{\max} \simeq 30\,\mathrm{K}$, but for $\sigma_\parallel = \sigma_\perp = 1\,\mu$m, the temperature increase reaches $\Delta T_{\max} \simeq 0.9 \times 10^5\,\mathrm{K} \simeq 8\,\mathrm{eV}$. However, in the ultrafast regime and in out-of-equilibrium condition with $T_e \gg T_i$, the conductivity is expected to differ significantly from the static value at room temperature. In Ref. M. W. C. Dharma-wardana *et al.*, Phys Rev E 96, 053206 (2017), the ultrafast conductivity of aluminum is $\sigma_{\mathrm{Al,uf}} \simeq 1 \times 10^6\,\Omega^{-1}\,\mathrm{m}^{-1}$. With this new conductivity value, the temperature increase is $\Delta T_{\max} \simeq 1100\,\mathrm{K} \simeq 0.1\,\mathrm{eV}$ for $\sigma_\parallel = \sigma_\perp = 5\,\mu$m and $\Delta T_{\max} \simeq 3.5 \times 10^6\,\mathrm{K} \simeq 300\,\mathrm{eV}$ for $\sigma_\parallel = \sigma_\perp = 1\,\mu$m.

From the above estimates and with a melting point at a temperature of 933.5 K for aluminum, we see that although aluminum may or may not melt for a beam with $\sigma_\parallel = \sigma_\perp = 5\,\mu$m, it will certainly melt for $\sigma_\parallel = \sigma_\perp = 1\,\mu$m. In this case, we can estimate the total volume of aluminum that can potentially be melt after radial heat transport. The total heat generated in a thickness l is:

$$Q_{\mathrm{heat}} = \int \frac{|\mathbf{j_b}|^2}{\sigma_{\mathrm{Al}}}\, dV dt = \frac{e^2 c N^2}{8\pi^{3/2}\sigma_\parallel \sigma_\perp^2} \frac{l}{\sigma_{\mathrm{Al}}} \tag{23}$$

and this energy can melt a maximal volume $V_{\max} = \pi R_{\max}^2 l$ satisfying $Q_{\mathrm{heat}} = (c_v \Delta T_{\mathrm{melt}} + l_{\mathrm{Al}}) V_{\max}$, where $l_{\mathrm{Al}} = 1.1 \times 10^9\,\mathrm{J\,m^{-3}}$ is the latent heat of fusion per unit volume and $\Delta T_{\mathrm{melt}} \simeq 640\,\mathrm{K}$ is the temperature increase needed to reach the melting point. We obtain for $R_{\max}$:

$$R_{\max} = \left[\frac{e^2 c N^2}{8\pi^{5/2}\sigma_\parallel \sigma_\perp^2} \frac{1}{\sigma_{\mathrm{Al}}(c_v \Delta T_{\mathrm{melt}} + l_{\mathrm{Al}})} \right]^{1/2} \tag{24}$$

Considering $\sigma_\parallel = \sigma_\perp = 1\,\mu$m again, we find that aluminum can be melt up to a radius of $R_{\max} \simeq 9\,\mu$m when considering the static value of the conductivity, or up to $R_{\max} \simeq 60\,\mu$m with the ultrafast value.

A second important contribution to the energy deposited in the foil comes from self-field reflection, or in other words to CTR absorption. Part of the electromagnetic energy in the beam self fields is deposited at the foil surface during reflection. For reflection of electromagnetic waves at visible wavelength, few percents is typically absorbed at the surface, but reflectivity/absorption is difficult to calculate in the ultraintense ultrafast regime, especially because in this case the conductivity is not well known (see discussion above). To take an upper limit corresponding to a worse case scenario, we assume that a fraction $f = 10\,\%$ of the EM energy in the self fields is deposited in the foil. The expressions of the self fields given in Eqs. (1)-(2) are valid for $r \lesssim \gamma\sigma_\parallel$, that is for $r \lesssim 20\,$mm for a 10 GeV electron beam with $\sigma_\parallel = 1\,\mu$m. Computing $W_{\rm EM,self}(R_{\max})$, the total EM energy in the self fields within $r \leq R_{\max}$, we can estimate how much volume can be melt in an aluminum foil of thickness l using the following equality:

$$fW_{\rm EM,self}(R_{\max}) = (c_v\Delta T_{\rm melt} + l_{\rm Al})\pi R_{\max}^2 l \tag{25}$$

For an aluminum foil with a thickness $l = 2\,\mu$m and for a 10 GeV electron beam with 2 nC of charge and $\sigma_\parallel = \sigma_\perp = 1\,\mu$m, we obtain $R_{\max} \simeq 0.9\,$mm, corresponding to a deposited energy $W_{\rm dep}(r \leq R_{\max}) = fW_{\rm EM,self}(R_{\max}) \simeq 13\,$mJ. For $\sigma_\parallel = \sigma_\perp = 5\,\mu$m, $R_{\max} \simeq 0.3\,$mm and the deposited energy is $W_{\rm dep}(r \leq R_{\max}) = fW_{\rm EM,self}(R_{\max}) \simeq 1.5\,$mJ. This worse case analysis shows that, considering only the deposited energy due to self-field reflection, the expected damage size in the foil is in mm scale. This does not include the effect of momentum transferred to the foil, which could potentially lead to a larger damage for very thin foils.

3 Numerical results

To assess the viability of NF-CTR beam focusing in multiple foils with current, or shortly available, FACET-II electron beam parameters, we have carried out a numerical campaign using CALDER-Circ with realistic parameters and considering different beam and target configurations. All of the simulations used the PIC code CALDER-Circ in a rotationally symmetric geometry [A. F. Lifschitz *et al.*, J. Comput. Phys. 228, 1803 (2009)]. The 10 GeV electron beam was initialized with 2 nC charge, 3 mm mrad emittance, 5 μm transverse beam size (rms), and either 1 μm or 5 μm bunch length (rms) to evaluate the robustness of the scheme to the beam current. The target consisted of a stack of 1-μm-thick aluminum foils with 100 μm vacuum gaps in between. In one case, the electron beam directly impinges on this foil stack, in another case, a single foil is placed 14 mm upstream of the foil stack to pre-focus the beam. Figure 4 shows the beam phase space after the first foil along with the evolution of the beam size in the scenario with single foil and following foil stack. The focusing effect is in good agreement with the analytical model (orange dashed line, based on Eq. 5) assuming reflection of the beam self-fields at the foil surface. The simulations also show that the beam focuses from 5 μm to $\sim$1.5 μm transverse beam size (rms) after the first foil, and to below 1 μm within the first few

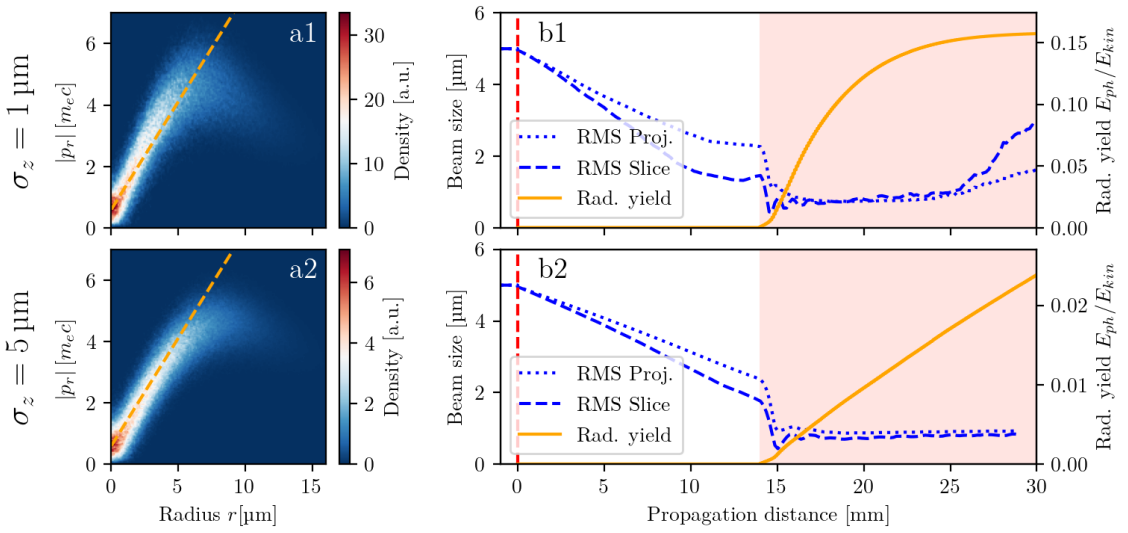

Figure 4: Rotationally symmetric PIC simulations of a 10 GeV, 2 nC and 100 kA electron beam with 1 μm and 5 μm rms bunch length (top and bottom row respectively), impinging on a single 1-μm-thick aluminum foil (dashed red line in b1/b2), followed by 14 mm of free propagation in vacuum, and a stack of foils separated by 100 μm vacuum gaps (red shaded area in b1/b2). The figures a1 and a2 show the phase space after the first foil with the solution of the analytical model (orange dashed line) from section 2.1. The figures b1 and b2 show the evolution of the beam size (projected and slice) and of the yield of gamma-ray radiation.

foils of the stack. The radiation yield reaches up to 16 % of the total beam energy for a 1-μm-long beam.

Figure 5 shows the evolution with propagation distance of the transverse beam size and the radiation yield, in the case where the beam directly impinges onto the foil stack. Here, also less optimistic beam parameters are considered: even with a 25 % reduced charge (0.5 nC), a percent-level radiation yield is obtained, which is expected to be clearly measurable in the FACET-II experiment. The simulations confirm the promising potential of the E-332 experiment at FACET-II, where the foils' surfaces of a foil stack is expected to focus the electron beam until it eventually reaches a density comparable to the solid density, during which large amounts of gamma rays are emitted and one can enter the SFQED regime. They show that the radiation mechanisms are robust enough to be measurable under various, shortly available configurations. This scheme would allow unprecedented electron and gamma-ray parameters to be achieved.

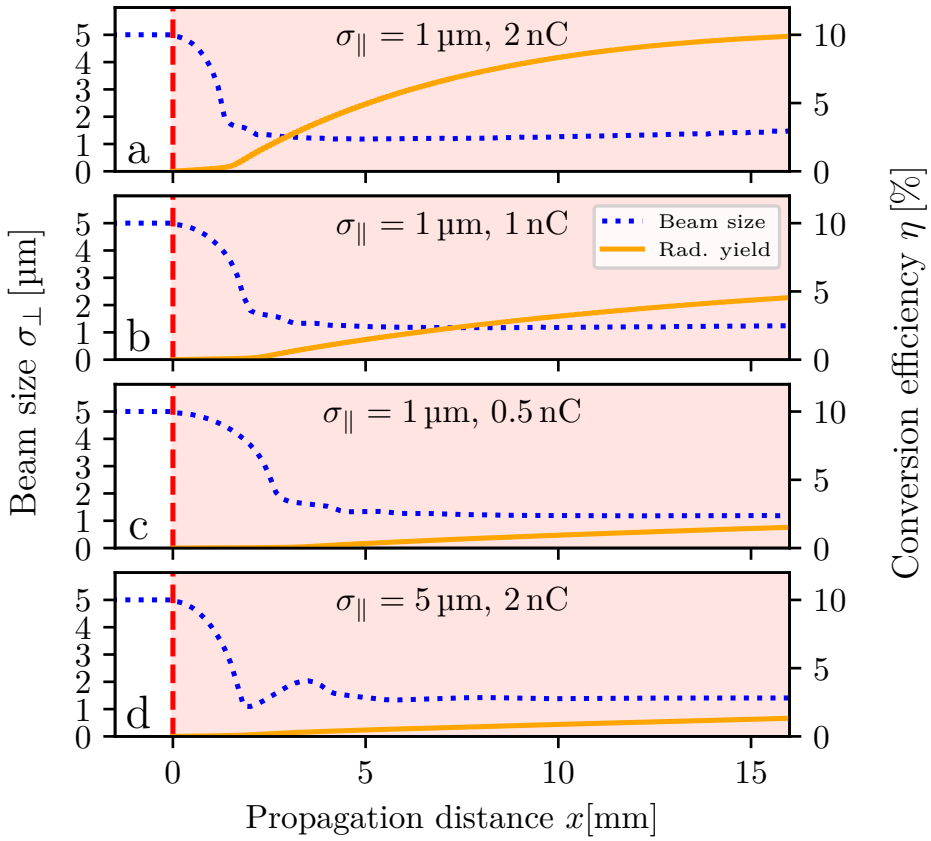

Figure 5: Rotationally symmetric PIC simulations of a 10 GeV electron beam with different bunch lengths and charges. The electron beam is impinging on a stack of 1-μm-thick aluminum foils starting at $x = 0$ (red shaded area), and separated by 100 μm vacuum gaps. Each figure shows the evolution of the beam size (projected) and of the yield of gamma-ray radiation. The conversion efficiency of the electron beam to radiated energy is above the percent level for all cases. Figure from the supplementary material of Ref. A. Sampath *et al.*, Phys. Rev. Lett. 126, 064801 (2021).